

Continuously tunable orbital angular momentum generation using a polarization-maintaining fiber

ROBERT D. NIEDERRITER,^{1,*} MARK E. SIEMENS,² AND JULIET T. GOPINATH^{1,3}

¹Department of Physics, University of Colorado, 390 UCB, Boulder, Colorado 80309-0390, USA

²Department of Physics and Astronomy, University of Denver, 2112 East Wesley Avenue, Denver, Colorado 80208, USA

³Department of Electrical, Computer, and Energy Engineering, University of Colorado, 425 UCB, Boulder, Colorado 80309-0425, USA

*Corresponding author: robert.niederriter@colorado.edu

Received 26 April 2016; revised 10 June 2016; accepted 13 June 2016; posted 14 June 2016 (Doc. ID 262844); published 7 July 2016

We demonstrate the generation of orbital angular momentum (OAM) in a two-mode polarization-maintaining (PM) optical fiber. We combine two linearly polarized modes of PM fiber to generate linearly polarized optical vortex beams with OAM. The average OAM can be finely varied by changing the phase between modes. We have quantitatively measured the resulting OAM to vary between $\pm 1\hbar$ per photon while varying the relative phase between the LP_{11e} - and LP_{11o} -like fiber modes. The modal purity is 97%. © 2016 Optical Society of America

OCIS codes: (060.2310) Fiber optics; (060.2420) Fibers, polarization-maintaining; (080.4865) Optical vortices; (140.3300) Laser beam shaping; (260.6042) Singular optics.

<http://dx.doi.org/10.1364/OL.41.003213>

Generation and control of the orbital angular momentum (OAM) of light has been an active area of research since OAM was identified in the azimuthal phase structure of laser beams with helical wavefronts [1]. The first demonstrations were based on mode conversion between Hermite–Gaussian (HG) and Laguerre–Gaussian (LG) beams using cylindrical lenses [2]. Simple and robust generation of OAM beams typically requires precision optical components such as spiral phase plates [3,4], spatial light modulators [5,6], or Q-plates [7,8], operated either internal or external to the laser cavity.

OAM generation using optical fiber has potential for applications in fiber communications, imaging, and sensing. The wavefront and OAM at the output of multimode optical fiber can be controlled by the launch conditions and bending of the fiber [9–11]. Measurement of the fiber transformation matrix and the principal modes enables wavefront shaping at the distal end of a multimode fiber by precise control of the input wavefront using a spatial light modulator. Shaping the output of multimode fiber shows promise for particle manipulation, endoscopy, and mode division multiplexing. Others have used the fiber itself as the wavefront shaping element for generation of OAM in optical fibers based on combinations of TE, TM, EH, and HE modes [12–16]. These annular fiber modes have an obvious connection to annular OAM beams, but they are difficult

to generate using commercial fibers, and their nearly degenerate propagation constants lead to strong modal coupling in standard step-index fiber. It is possible to generate radial- and azimuthal-polarization vector beams by precise off-axis coupling in a short, straight two-mode step-index fiber [13,14], but the technique appears limited by mode mixing in long, coiled fiber [15] and the mode purity has not been characterized.

The generation of OAM in polarization-maintaining (PM) optical fibers has not been explored. The birefringence of PM fiber breaks the circular symmetry of the fiber modes which offers several advantages for generating OAM. First, PM fiber supports linearly polarized eigenmodes, approximately equal to the LP modes of the weakly guiding approximation, and allows the generation of linearly polarized OAM modes. Numerical simulations of the modes of PM fiber (based on [17]) show that the eigenmodes are linearly polarized with a polarization ratio of better than 40 dB. The higher-order modes of PM fiber provide a convenient basis set with the same azimuthal structure as Hermite–Gaussian modes. We will refer to the PM fiber eigenmodes as PM_{lpe} and PM_{lpo} , where l and p are azimuthal and radial mode indices, respectively, and subscripts e and o refer to even and odd azimuthal dependence of the electric field, respectively. Second, the large birefringence of PM fiber lifts the degeneracy of the fiber modes and greatly reduces coupling between modes of orthogonal polarization. Preventing mixing between polarization states is beneficial in many applications and allows the use of long, coiled fibers. In addition, PM fibers may be especially interesting as OAM-based fiber optic sensors [18]. In this Letter, we report on the generation and control of vortex beams in coiled 2 m long two-mode PM optical fibers.

Generation of OAM modes in PM fiber follows the same technique as mode conversion between Hermite– and Laguerre–Gaussian beams [1,2]. In a typical mode converter, the electric fields corresponding to two HG modes are combined with a $\pi/2$ phase delay to generate a LG mode with OAM:

$$HG_{10} + iHG_{01} = LG_{01}. \quad (1)$$

The equation can be generalized by the following for modes with the same $\cos\theta$ and $\sin\theta$ azimuthal dependence but arbitrary radial dependence, $f(r)$, where (r, θ) are radial and azimuthal coordinates:

$$f(r) \cos \theta + if(r) \sin \theta = f(r)e^{i\theta}. \quad (2)$$

The PM_{11e} and PM_{11o} fiber modes exhibit the same $\cos \theta$ and $\sin \theta$ azimuthal structure as HG modes, so they can be combined to form beams with OAM. Regardless of the radial function, $f(r)$, the relative phase, $\Delta\phi$, between the even and odd (sine and cosine) modes determines the generated OAM. For the general case, $f(r) \cos \theta + \exp(i\Delta\phi)f(r) \sin \theta$, the average OAM per photon is equal to $\sin(\Delta\phi)$.

We have demonstrated the generation of OAM-carrying donut beams in two-mode PM optical fiber. The experimental results in Fig. 1 show the generation of an OAM mode from the combination of PM_{11} modes with $\pi/2$ relative phase. When the relative phase is 0, the fiber output has zero average OAM.

A schematic of the experiment is shown in Fig. 2. We used a 2 m long PM980-XP fiber (Nufern), with birefringence of $\sim 3.5 \times 10^{-4}$. The fiber is designed to be single mode at 980 nm; at 633 nm, it supports the PM_{11} mode group as well as the PM_{01} mode (six modes total, including the polarization multiplicity).

We couple light from a He-Ne laser (632.8 nm) into the PM_{11e} and PM_{11o} modes using a Mach-Zehnder interferometer aligned such that each of the two beams couples into only the even or odd PM_{11} mode; one incident beam is focused into the fiber with slight horizontal displacement from the fiber axis to generate PM_{11e} , while the other beam is displaced vertically to generate PM_{11o} . The alignment of each beam is separately optimized for generation of pure PM_{11} modes at the output. The

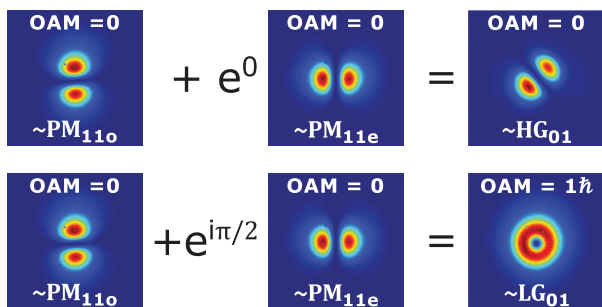


Fig. 1. Experimental intensity profiles of individual PM fiber modes, PM_{11e} and PM_{11o} , and the resulting mode, either $\sim HG_{01}$ or $\sim LG_{01}$, depending on the relative phase between the fiber modes.

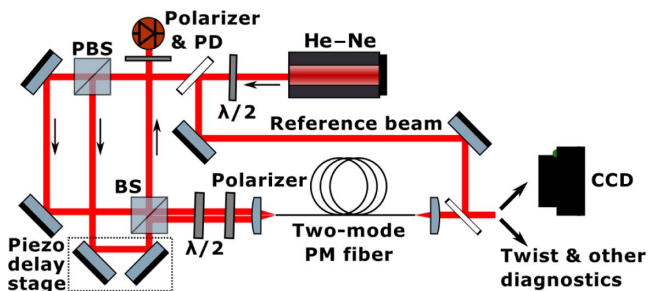


Fig. 2. Experimental schematic for generating OAM via mode addition in PM fiber. He-Ne, helium-neon laser (632.8 nm); $\lambda/2$, half-wave plates; PBS, polarizing beam splitter; BS, nonpolarizing beam splitter; PD, photodetector. The polarizers are oriented at 45° to combine the horizontal and vertical polarizations with equal amplitudes.

individual PM_{11} modes are shown on the left-hand side of Fig. 1. Adjusting the relative phase between the excitation beams using a piezo-driven delay stage controls the generated OAM.

The fiber polarization axes at the input are aligned to the input polarization. The output end of the fiber is rotated so that the polarization axes are aligned at 45° to the optical table because this leads to horizontal- and vertical-oriented HG-like modes when the relative phase is zero and π , respectively.

The two input modes are the same linear polarization, though the scheme could be easily modified to use alternative input polarizations. The output polarization ratio is better than 20 dB, which is the specification of the PM fiber. The individual PM mode shapes, powers, and polarizations do not change when bending or heating the fiber, indicating that the excited modes are the eigenmodes.

As a preliminary measurement of the helical phase generated, we interfered the fiber output with a reference beam. Figure 3 shows the spiral interference patterns which indicate helical phase structure. A 100 mm focal length spherical lens was added in the reference arm to produce a clear spiral pattern. When the relative phase between PM fiber modes is $\pi/2$, the OAM is positive and the spiral is counterclockwise; when the relative phase is $-\pi/2$, the OAM is negative and the spiral is clockwise; when the relative phase is zero, the OAM is zero and no spiral is formed. The spiral interference patterns indicate that the beam carries orbital angular momentum, though it is difficult to quantify the angular momentum based on interference measurements alone.

Quantitative measurements of orbital angular momentum typically require complicated or custom apparatuses, such as Dove prism arrays [19], holograms [20], Shack-Hartmann wavefront sensors [21], or custom phase masks [22,23]. In contrast, we have chosen a relatively simple method for the single-shot absolute measurement of the OAM based on the twist parameter. This technique is familiar in the characterization of general astigmatic laser beams [24–26]. For comparison, we also measured the mode purity with a forked hologram method.

Measurements of the twist parameter require only a cylindrical lens and a beam profiling device such as a CCD. A beam-carrying OAM will rotate after passing through a cylindrical lens, which indicates the presence of OAM. The average OAM can be measured by calculating the xy covariance of the intensity distribution [24] as

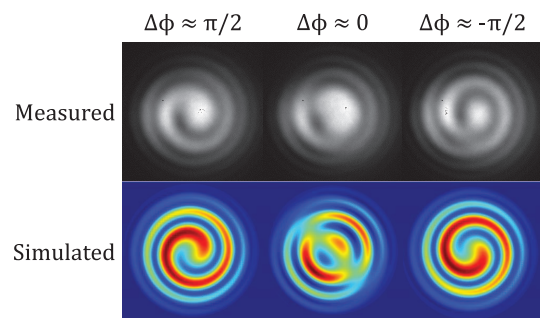


Fig. 3. Qualitative measurement of orbital angular momentum by interference with a reference beam. The relative phase, $\Delta\phi$, was varied using a piezo-controlled delay stage.

$$\langle xy \rangle = \frac{\iint I(x, y)(x - \langle x \rangle)(y - \langle y \rangle) dx dy}{\iint I(x, y) dx dy}, \quad (3)$$

where x and y are the spatial coordinates in the plane of the CCD, and $\langle x \rangle$ and $\langle y \rangle$ describe the location of the centroid of the intensity distribution, $I(x, y)$.

A variety of factors such as the beam divergence and asymmetries in the initial intensity distribution can cause errors in the OAM measurement. Measuring instead the difference between $\langle xy \rangle$ under horizontal- and vertical-focusing conditions avoids the need for precise collimation of the beam [27]. The OAM measured using this scheme is given by

$$L_{\text{Ave}} = \hbar \frac{2\pi f}{\lambda d^2} (\langle xy \rangle_v - \langle xy \rangle_h), \quad (4)$$

where L_{Ave} is the average optical orbital angular momentum, f is the cylindrical lens focal length, d is the lens-camera separation distance, λ is the wavelength, and v and h indicate the covariances measured after vertically and horizontally focusing cylindrical lenses, respectively.

To measure the OAM quickly, we developed a scheme to simultaneously measure the covariance in both the horizontal- and vertical-focusing conditions using two cylindrical lenses mounted at right angles to each other one focal length from a CCD, as shown in Fig. 4. The beam images in Fig. 4 slightly deviate from ideal due to imperfections in the optics and minute misalignments; these deviations are small and have little effect on the measured OAM.

The precise angle between the two lenses needed to be calibrated as the twist measurement technique is very sensitive to the rotation of the cylindrical lenses. For calibration, we compared the measured and expected OAM after a vortex phase plate (VPP-1a, RPC Photonics) was used to generate $l = \pm 1$ or 0 states and made slight adjustments to the cylindrical lens rotation to ensure an accurate measurement. After calibration, there was an overall shift in the measured OAM of $\sim 0.03 \hbar/\text{photon}$. The relative accuracy of the measurements is estimated to be better than $0.01 \hbar/\text{photon}$ based on measurements of pure OAM modes generated with vortex phase plates. The twist measurements are highly repeatable; the standard deviation of 30 measurements is typically between 0.001 and 0.003 \hbar/photon .

To verify the sinusoidal dependence of OAM with phase between fiber modes, we measured the OAM as a function of delay between the two modes. We measured the relative phase of the modes independently from the OAM based on the interference between the two beams before the fiber. The interference pattern included several bright and dark

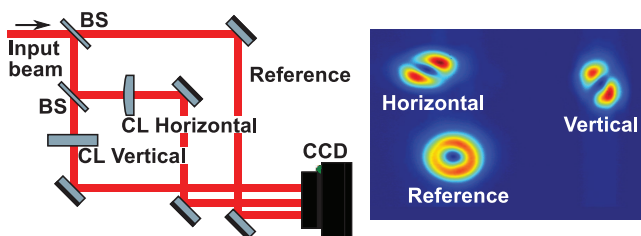


Fig. 4. Twist measurement scheme for real-time determination of the average orbital angular momentum based on two cylindrical lenses (labeled “CL Horizontal” and “CL Vertical”). Horizontally and vertically focused beams are both recorded on a camera one focal length away as well as a reference beam that does not pass through any cylindrical lenses.

fringes due to noncollinear alignment between the two beams required for off-axis coupling into distinct fiber modes. A small photodiode captured light primarily from a single bright or dark fringe of the interference pattern. The photodiode registered the change in intensity as the fringes shifted due to the piezo motion. The relative phase (with an arbitrary offset) was calculated by fitting a sine function to the measured interference signal. A detector after the fiber verified the power coupled into the fiber was not changing as a result of the piezo motion, resulting in a pure phase shift.

The measured average OAM oscillates as the relative phase between modes changes (Fig. 5). The OAM oscillations have a period of $(2 \pm 0.02)\pi$, which matches very well to theory and demonstrates the sensitivity of the OAM to small changes in phase between the constituent fiber modes. The peak-to-peak OAM is $(1.99 \pm 0.02) \hbar/\text{photon}$. The OAM maxima and minima are 0.97 and $-1.02 \hbar/\text{photon}$, respectively, which is consistent with a small overall shift of the measured OAM. It is interesting to note that the points with zero average OAM are equal superpositions of $+1$ and -1 OAM states.

The OAM mode purity was measured by decomposing the generated beam directly after the PM fiber into the constituent OAM modes. The first-order diffraction of a beam from a forked grating of order l has an added helical phase, $\exp(i l \theta)$. The Fourier transform contains the correlation between the helical phase and the beam under test. The modal contribution of each OAM mode is measured by recording the power in the center of the beam profile in the Fourier plane [4,20,28–30]. The hologram-based mode content measurement schematic is shown in Fig. 6. A computer-controlled reflective phase-only liquid crystal spatial light modulator was used to generate the holograms. A transform lens and aperture transmits only the first diffraction order, and a long focal length lens images the far-field beam profile onto the CCD with magnification to improve the resolution. We applied a series of phase-only forked grating patterns

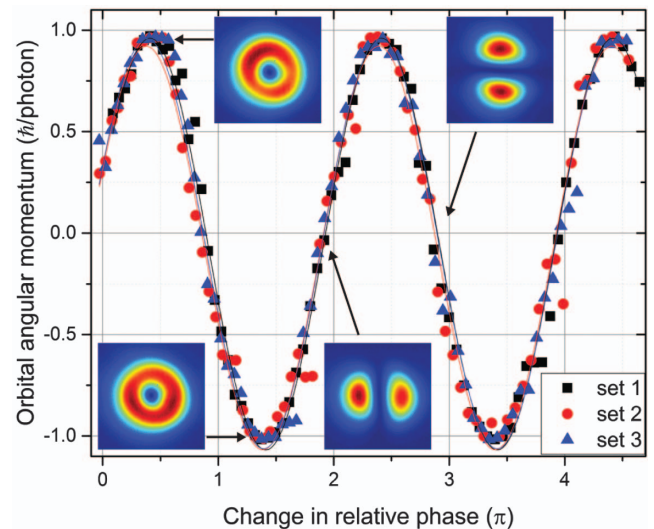


Fig. 5. Average orbital angular momentum per photon as a function of the relative phase, $\Delta\phi$, between modes controlled by the delay stage. Three independent trials with sinusoidal fits show that the average OAM oscillates as expected with a period of 2π , within the measurement uncertainty. The peak-to-peak OAM is $1.99 \pm 0.02 \hbar/\text{photon}$. The uncertainty in each measurement is smaller than the symbols.

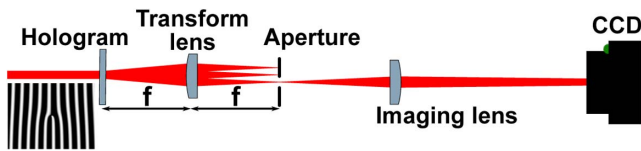


Fig. 6. Measurement scheme for OAM mode purity measurements. A series of forked holograms is applied using a spatial light modulator, and the modal power is quantified by the power in the center of the far-field beam profile recorded with a CCD.

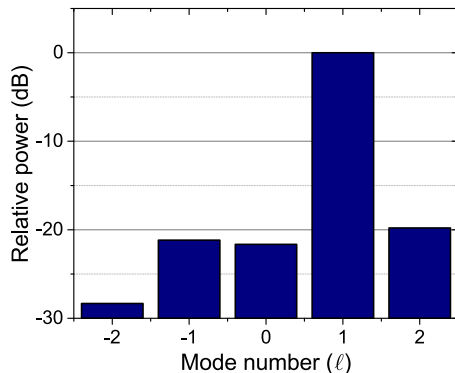


Fig. 7. Representative data set showing the high mode purity of the generated OAM beams, corresponding to a beam of primarily $l = 1$ OAM mode. The average OAM was calculated to be $0.99 \hbar/\text{photon}$ from the measured modal powers, with less than 1% of the power in each other mode.

corresponding to $l = -2, -1, 0, +1, +2$. The power in the center of the beam profile in each case corresponds to the amount of power in the conjugate OAM mode.

The measured OAM mode purity is 97%. A representative data set is shown in Fig. 7, corresponding to a beam of primarily $l = 1$ OAM mode. In this case, the average OAM was calculated to be $0.99 \hbar/\text{photon}$ from the measured mode content. Less than 1% of the power is in any other mode, and less than 3% of the power is in all modes other than the primary mode. The CCD camera noise limits the mode content measurements to $\sim 0.1\%$ (-30 dB). The estimated uncertainty of the mode content measurements is $\sim 1\%$ (-20 dB), primarily due to aberrations inherent in the low-cost spatial light modulator [31].

In conclusion, we have demonstrated the generation of OAM modes in 2 m of coiled PM optical fiber. The same degree of control is expected with longer fiber, as mode coupling is minimized. Off-axis coupling into the higher-order PM_{11} -like eigenmodes of PM fiber forms OAM beams and allows fine tuning of the OAM produced. The OAM mode purity is about 97%, with less than 1% of the power in any other OAM mode. Varying the relative phase between fiber modes causes sinusoidal oscillations in the average OAM between $\pm 1 \hbar/\text{photon}$, as predicted. A source of tunable average OAM has potential uses in sensing and imaging.

Funding. National Natural Science Foundation of China (NSFC) (ECCS 1509733, 1509928); U.S. Department of Defense (DOD), NDSEG Fellowship.

Acknowledgment. The authors are grateful for technical discussions with Dr. Martin Lavery (University of Glasgow), Samuel Alperin (University of Denver), Trystan Binkley-Jones, and Brendan Heffernan (University of Colorado Boulder) as well as loans of a vortex phase plate from Dr. Stephanie Meyer and Dr. Emily Gibson (University of Colorado Denver, Anschutz Medical Campus) and a wavefront sensor from Dr. Robert McLeod (University of Colorado Boulder).

REFERENCES

1. L. Allen, M. W. Beijersbergen, R. J. C. Spreeuw, and J. P. Woerdman, *Phys. Rev. A* **45**, 8185 (1992).
2. M. W. Beijersbergen, L. Allen, H. E. L. O. van der Veen, and J. Woerdman, *Opt. Commun.* **96**, 123 (1993).
3. M. W. Beijersbergen, R. P. C. Coerwinkel, M. Kristensen, and J. P. Woerdman, *Opt. Commun.* **112**, 321 (1994).
4. H. Li, D. B. Phillips, X. Wang, Y.-L. D. Ho, L. Chen, X. Zhou, J. Zhu, S. Yu, and X. Cai, *Optica* **2**, 547 (2015).
5. S. Ngcobo, I. Litvin, L. Burger, and A. Forbes, *Nat. Commun.* **4**, 2289 (2013).
6. P. Gregg, P. Kristensen, and S. Ramachandran, *Optica* **2**, 267 (2015).
7. L. Yan, P. Gregg, E. Karimi, A. Rubano, L. Marrucci, R. Boyd, and S. Ramachandran, *Optica* **2**, 900 (2015).
8. D. Naidoo, F. S. Roux, A. Dudley, I. Litvin, B. Piccirillo, L. Marrucci, and A. Forbes, *Nat. Photonics* **10**, 327 (2016).
9. T. Čižmar and K. Dholakia, *Nat. Commun.* **3**, 1027 (2012).
10. J. Carpenter, B. J. Eggleton, and J. Schröder, *Opt. Express* **22**, 96 (2014).
11. M. Plöschner, T. Tyc, and T. Čižmar, *Nat. Photonics* **9**, 529 (2015).
12. T. Grosjean, A. Sabac, and D. Courjon, *Opt. Commun.* **252**, 12 (2005).
13. N. K. Viswanathan and V. V. G. K. Inavalli, *Opt. Lett.* **34**, 1189 (2009).
14. V. K. Inavalli and N. K. Viswanathan, *Opt. Commun.* **283**, 861 (2010).
15. S. Ramachandran and P. Kristensen, *Nanophotonics* **2**, 455 (2013).
16. Z. Q. Fang, Y. Yao, K. G. Xia, M. Q. Kang, K. Ueda, and J. L. Li, *Opt. Commun.* **294**, 177 (2013).
17. A. B. Fallahkhair, K. S. Li, and T. E. Murphy, *J. Lightwave Technol.* **26**, 1423 (2008).
18. R. D. Niederriter, M. E. Siemens, and J. T. Gopinath, "Fiber optic sensors based on orbital angular momentum," in *CLEO: 2015* (Optical Society of America, 2015), paper SM1L.5.
19. J. Leach, M. J. Padgett, S. M. Barnett, S. Franke-Arnold, and J. Courtial, *Phys. Rev. Lett.* **88**, 257901 (2003).
20. S. J. Parkin, T. A. Nieminen, N. R. Heckenberg, and H. Rubinsztein-Dunlop, *Phys. Rev. A* **70**, 023816 (2004).
21. J. Leach, S. Keen, M. J. Padgett, C. Saunter, and G. D. Love, *Opt. Express* **14**, 11919 (2006).
22. G. C. G. Berkhout, M. P. J. Lavery, J. Courtial, M. W. Beijersbergen, and M. J. Padgett, *Phys. Rev. Lett.* **105**, 153601 (2010).
23. M. P. J. Lavery, D. J. Robertson, A. Sponselli, J. Courtial, N. K. Steinhoff, G. A. Tyler, A. E. Willner, and M. J. Padgett, *New J. Phys.* **15**, 013024 (2013).
24. J. Serna, F. Encinas-Sanz, and G. Nemes, *J. Opt. Soc. Am. A* **18**, 1726 (2001).
25. R. D. Niederriter, M. E. Siemens, and J. T. Gopinath, *Appl. Opt.* **52**, 1591 (2013).
26. S. N. Alperin, M. E. Siemens, R. D. Niederriter, and J. Gopinath, "Measuring orbital angular momentum of light with a single, stationary lens," in *CLEO: 2015* (Optical Society of America, 2015), paper JTu5A.14.
27. "Part 2: general astigmatic beams," ISO 11146-2:2005 (2005).
28. T. Kaiser, D. Flamm, S. Schröter, and M. Duparré, *Opt. Express* **17**, 9347 (2009).
29. D. Flamm, D. Naidoo, C. Schulze, A. Forbes, and M. Duparré, *Opt. Lett.* **37**, 2478 (2012).
30. I. A. Litvin, S. Ngcobo, D. Naidoo, K. Ait-Ameur, and A. Forbes, *Opt. Lett.* **39**, 704 (2014).
31. D. Huang, H. Timmers, A. Roberts, N. Shivaram, and A. S. Sandhu, *Am. J. Phys.* **80**, 211 (2012).